Machinability Analysis on Laser Sintered Materials with Finite Element Method

Ahmad Shahir Jamaludin, Abdullah Yassin

Abstract— **The term machinability of workpiece materials relates to the easiness of a metal to be machined to an adequate surface finish. This paper clarified the analysis of laser sintered material machinability with mean of predicted cutting force and temperature distribution. 2D orthogonal cutting was employed on edge design tools with updated Lagrangian coupled thermo mechanical plane strain model. Adaptive meshing, tool edge radius and various types of friction models were assigned to obtain precise cutting results. Cutting force and cutting-edge temperature estimated by FE analysis are validated against corresponding experimental values by previous researchers. From the study, cutting force increases when radial depth increases and lowest error acquired when the shear friction factor of 0.8 was applied. Machining simulation for laser sintered materials estimated lower cutting force compared to mild steel AISI1055 due to lower Young modulus. Higher cutting temperature estimated for machining simulation laser sintered material compared to machining simulation mild steel AISI1055 due to its low thermal conductivity.**

***Index Terms*— Finite element method (FEM), 2D orthogonal end milling, cutting force prediction, cutting temperature prediction, friction model**

I. Introduction

Injection moulding is one of the most flexible and prominent operations for mass manufacture of complicated plastic parts with excellent dimensional tolerance. In the conventional mould manufacturing, mould is prepared from the hardened steel using subtractive processes such as high speed machining (HSM) [1] and electro discharge machining (EDM) [2]. These processes are time consuming; therefore, the conventional mould manufacturing is not economic. In additional, in making a precise mould having a deep rib, tool deflection could cause various negative effects such as chatter, wobble and impact. This issue will result in poor dimensional accuracy.

Ahmad Shahir Jamaludin is with the Universiti Malaysia Sarawak, Kota Samarahan, 94000, Sarawak, Malaysia (corresponding author phone: 082-583246 ; e-mail: aero_zephyr@yahoo.com).

Abdullah Yassin is with Department of Mechanical and Manufacturing Engineering, Universiti Malaysia Sarawak, Kota Samarahan, 94300, Sarawak, Malaysia. (E-mail: yabdulla@feng.unimas.my).

Reducing tool length is one of the ways to control the tool deflection but capability to produce deep rib on the mould reduces. Hence, conventional mould manufacturing is unsuitable in production of complicated injection mould.

Application of stereolithography (SL) techniques has decreased time and cost of mould manufacturing [3]. Moreover, deep rib on a mould can be produced. Still, due to its low flexural stresses, life span of the mould produce from SL is short [3]. Introducing Selective Laser Sintering (SLS) where the application of a laser beam to irradiate metal powder in making three dimensional shaped parts. This technique could greatly lessen mould manufacturing time and increase its life span. However, resulting part offers limited accuracy and poor surface roughness [4].

These deficiencies were overcome by invention of milling-combined laser sintering system (MLSS), which integrates laser sintering of fine metallic powder with high speed machining. Ball end mill with a small or micro diameter is employed to machine complex mould features. This is because the ball end mill capable in machining free-form surfaces [5]. Therefore, making deep ribs on complicated mould is achievable and the dimensional accuracy is also enhanced. About, 30% from the total production time is required for high speed machining (HSM) in making a mould. It is critical to comprehend the machinability of the laser-sintered material, where cutting the laser-sintered material effectively is one of the important factors in gaining utmost economic benefit from MLSS.

According to S. Kalpakjian [4], machinability of workpiece materials refers to the reduced difficulty with which a given metal can be machined to an acceptable surface finish. Materials with good machinability require less cutting force, low processing time, acquirable better surface finish, and cause small gradual failure on cutting tool.

Surprisingly, fewer concerns were given by the researchers on machinability study of laser-sintered material [6]. According to experimental studied that been done by A.Yassin *et al*., laser sintered material can be considered as difficult to machine. This is due to its low thermal conductivity, and high material hardness. Since, laser sintered material is powder metallurgical base material, its porousness causes it hard to obtain satisfactory surface roughness, although low cutting force needed to cut the materials [6]. Hence, machinability study on laser sintered material is a key factor in gaining the advantage of MLSS as a new invention in mould making.

In this study, machinability of laser-sintered material was analyzed with mean of cutting force and cutting temperature generated on the cutting tool during the machining process by FE simulation. In addition, comparison with the machining processes by FE simulation for mild steel; AISI1055 was also been done.

II. Finite Element Method (FEM)

Finite element method (FEM) is a numerical solving technique by dividing a problem into small finite regions called elements. Finite element method (FEM) has become distinguished in simulating high speed machining and beneficial in saving cost, time, and capable of forecast effects of cutting parameter on cutting force, cutting-edge temperature and chip formations [7,8]. With the implementation of FEM, cutting forces and temperatures acquired can be used in estimating the ideal cutting conditions such as cutting speed, cutting depth, etc.

One of the most simplified models of FEA for machining is 2D orthogonal cutting. Orthogonal cutting involved cutting edge moves perpendicular to the relative motion between cutting tool and workpiece to remove unwanted material from the workpiece with constant uncut chip thickness [7]. The earlier researchers developed 2D orthogonal cutting such as Usui and Shirakashi obtained steady state cutting using iterative convergence method in FEM [9]. Strenkowski and Carroll developed numerical model without a preformed chip using updated Lagrangian code [10]. In these models, effect of uncut chip thickness was neglected since 2D orthogonal cuttings were common in simulating turning processes. In favor of milling operation, uncut chip thickness inconstant, depends on fix parameters of radial depth, cutting tool diameter and cutting feed and cutting-edge position [8].

Current 2D model developed by L. Filice *et al.* [7] and T. Özel [8], applied friction condition in acquiring more useful data. J.P. Davim *et al.* studied plastic strain and plastic strain rate in machining AISI1045 FEM simulation to observe its effect in cutting process [11]. Updated Lagrangian formulation on 2D thermo mechanical plane strain FEM model will be assigned for the study.

In this study, laser sintered material will be applied as main material properties and AISI1055 will be the comparison. Previously, A. Yassin and T. Furumoto *et al.* studied the machinability of laser-sintered materials [6, 15, 16] experimentally without FEM analysis. Therefore, application of FEM could extend the knowledge of MLSS and laser sintered material.

III. Methodology

A. Finite element model

The 2D orthogonal finite-element models were developed base on the ball end mill geometry from the experimental study by A. Yassin, Figure 1[6]. Previous FEM machining models that been developed by L. Filice et al. and T. Özel also inspire this 2D FEM model [7, 8]. The model was developed only for a small part from the tool where the main contact between tool and workpiece occur. Table 1 show the summarization of the cutting tool characteristic in this study.

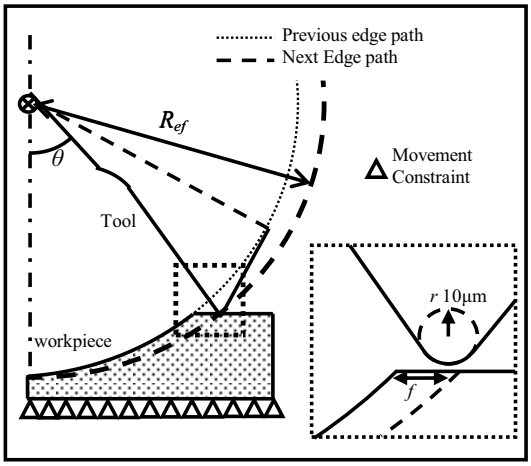

Figure 1: Simplified tool and workpiece FEM model

Table 1: Cutting tool geometry

Tool diameter, D [mm]	6.0
Tool maximum effective radius of revolution, R_{ef} [mm]	3.0
Tool rake angle, α [°]	5.0
Tool clearance angle, γ [°]	12.0
Tool edge radius, r [mm]	0.01
Feed rate, f [mm/tooth]	0.01

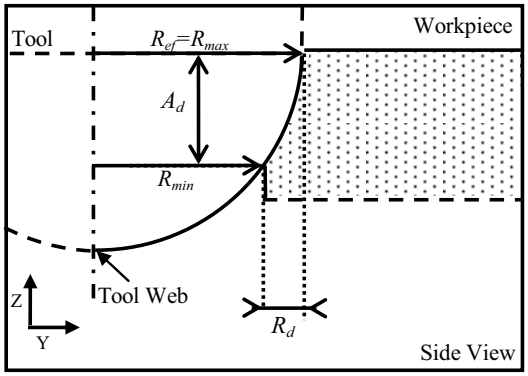

Figure 2: Peripheral milling on side view

In 2D analysis, complex ball part of the end mill was simplified where the maximum effective radius, R_{ef} was considered as the cutting tool rotation radius in acquiring cutting force and cutting temperature prediction. The size of rotation radius relies on the type of ball end milling procedure during the experiment. Figure 2 shows the diagram of the peripheral milling process.

In this study, the tool geometry was adjusted to the experimental approach of peripheral milling by A. Yassin *et al.* [6]. Peripheral milling is the process where teeth located

on the periphery of the cutter body generates the milled surface.

Commercially available FE software capable of executing isoparametric quadrilaterals meshing and adapted remeshing technique was applied. This type of mesh provides low element requirements and arbitrarily rotatable [17]. Adapted remeshing technique was applied where this technique able to remeshing the model if critical element distortion existed during the simulation [7, 8].

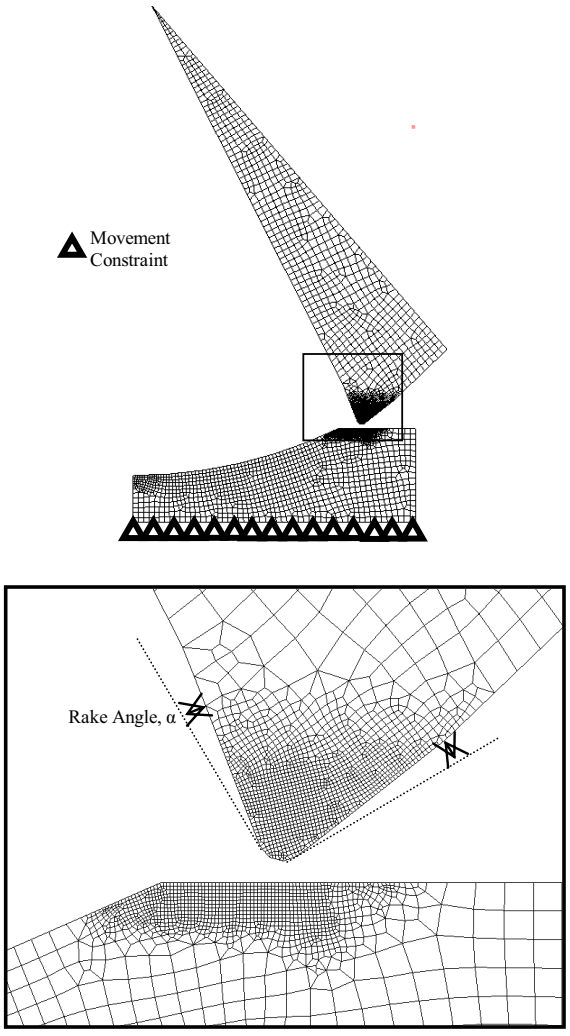

Figure 3: Model meshing and density

Denser and fine meshes were only assigned at the tool edge – workpiece contact area where main mechanical work and large elastic-plastic deformation were generated. This meshing method will ensure lighter and precise simulations can be done for the investigation. 2000 elements were use for workpiece, and 1000 elements were use for cutting tool mesh. Figure 3 shows an example of isoparametric quadrilaterals mesh with mesh density control that was applied in this study

Following are the assumptions made to simulate the complex procedure of metal cutting with FEM.

a) Contact Length

Eq.1 shows contact length model was use as tool-workpiece contact length assumption in the simulation, base Kato *et al.* [18], where L_c is tool-workpiece contact length and h in the undeformed chip thickness.

$$L_c = 2h \tag{1}$$

b) Constant Friction

Constant friction was assumed for all interaction between tool-chip and tool-workpiece. The type of friction model used in this study is called shear friction model. Frictional stress on rake face of tool is assumed constant and low stress variation of frictional stress, τ and normal stress, σ_n are neglected [8]. This can be expressed with following Eq. 2.

$$\tau = mk \tag{2}$$

m is friction factor from 0.6 to 0.9 (will be used in this study) and k is shear flow stress of the work material.

c) Heat Generation

Heat generation due to metal cutting Q_r (W) is equal to the rate of energy consumption during metal cutting, (Eq. 3) and separated between tool, workpiece and chip.

$$Q_r = W_c = F_v V \tag{3}$$

F_v (N) is the cutting force and V (m/sec) is the cutting speed. Heat flux, q (W/mm^2) may be acquired from the simulation as Eq. 4 [20].

$$q = Q_r / L_c b \tag{4}$$

b (mm) are contact length and cutting width.

d) Thermal Boundaries

Thermal boundary conditions are critical in calculating the temperature distribution in metal cutting simulation. In Figure 3, C'-C" defined the contact between the tool and the workpiece is assumed thermally perfect and a large value of h=1000 (kW/m^{2}K) is employed according to N.A. Abukhshim *et al.* [21].

Heat loss due to convection at the free surface of the tool and workpiece is defined to be caused by convection. The heat convection coefficient of 20 (W/m^{2}K) is employed to B-C', C"-A, H-D and D-E, according to L. Filice *et al.* [7].

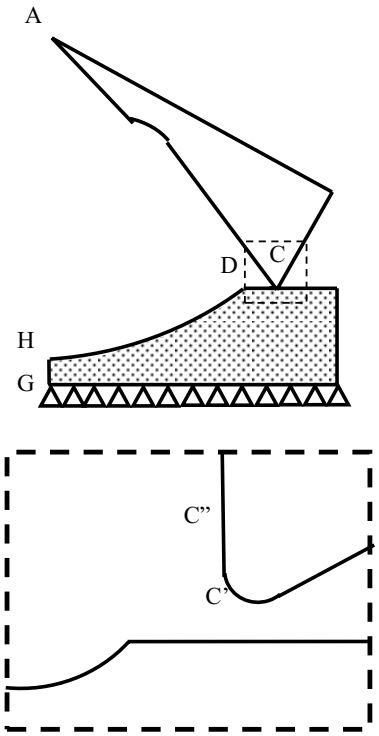

Figure 4: Thermal boundaries on tool and workpiece

The boundary sufficiently far apart from the cutting zone is assumed to be uninfluenced by cutting temperature and thus, boundaries A-B, E-F and F-G are fixed with environment temperature, 20 (^{o}C) according to N.A. Abukhshim et al. [21]. Heat loss due to radiation is neglected.

e) Data Collections

In validating the estimated cutting edge temperature with the experimental results, air cutting time and cooling effect have to be taken into account. According to A. Hosokawa *et al.*, the temperature at a given time after the tool finishes cutting the workpiece is given by Eq. 5.

$$T_{\psi}(\delta)=(T_r-T_0)e^{-a\delta}+T_r \quad (5)$$

T_{ψ} (^{o}C) is the temperature at a given air cutting time, T_r (^{o}C) is the instantaneous cutting temperature after tool finishes cutting the workpiece, δ (s) is the air cutting time, T_0 is the room temperature and a=0.3 is cooling constant which is determined from A. Hosokawa *et al.* [22]. Experimental results by A. Yassin *et al.* [6] measured by optical fiber was positioned at 180° from the cutting exit as shown in Figure 5.

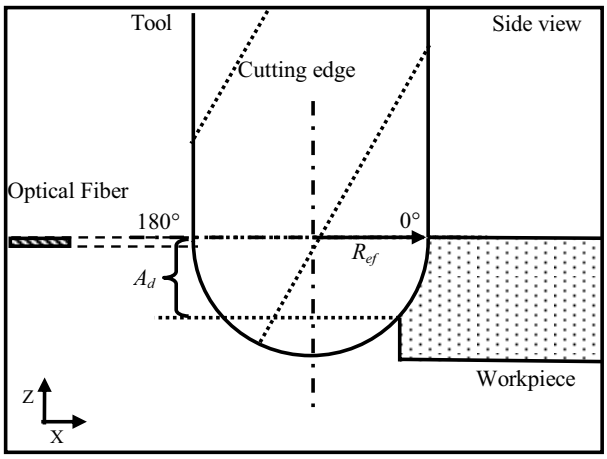

Figure 5: Temperature Measurement Schematic

B. Cutting Condition and Materials Properties.

The laser sintered material properties were taken for the inner surface of work material where metallic powder is fully melted due to heat and reheat process, which is 1.0 [mm] from the periphery surface according to A. Yassin *et al* [6]. Value of material hardness was increases from 211 ($HV_{0.3}$) to 275 ($HV_{0.3}$) when metallic powder was sintered with low energy density, 2.0 (J/mm^2) to medium energy density, 9.0 (J/mm^2). In addition, the value for material density also shows increasing value from 6950 (kgm^{-3}) to 7680 (kgm^{-3}). Nonetheless, nearly identical value of material hardness, 270 ($HV_{0.3}$) and density 7680 (kgm^{-3}) acquired when the metallic powder was sintered with high-energy density, 20 (J/mm^2).

Table 2 shows characteristic morphology of metallic powder, before it was sintered with medium energy density, 9.0 (J/mm^2) to form laser sintered material, LSMeρ9. Materials properties and cutting conditions are shown in Tables 3 and 4 [16, 17].

Table 2 Properties of metallic powder

Materials	SCM	Ni	Cu
Powder Density (kg/m^3)	4690	4040	4690
Specific Heat (J/kgK)	450	490	380
Thermal Conductivity (W/mK)	0.13	0.17	0.17
Particle Diameter (μm)	30	30	30
Percent of Composition (%)	70	20	10

SCM : Chrome Molybdenum Steel

Table 3 Tool and workpiece material properties

Materials	WC (Tool)	LSMEρ9	AISI1055
Young Modulus, E (GPa)	650	124	250
Poisson Ratio, ε	0.25	0.3	0.3
Thermal Conductivity, k (W/mK)	15	10	53
Density, ρ (kg/m^3)	14900	7680	7850
Specific Heat, c (J/kgK)	334	450	486
Hardness Vickers, $HV_{0.3}$	1400	275	145

Table 4 Cutting Conditions

Cutting tool diameter, D (mm)	0.6,1.0,2.0,6.0
Radial depth of cut, R_d (mm)	0.1-0.6
Revolution Speed (RPM)	4000-40000
Cutting speed, V_c (m/min)	75-754
Cutting feed, f (mm/tooth)	0.01

IV. Results and Discussion

FEM estimated cutting force and cutting edge temperature in the study are validated against corresponding experimental values by A. Yassin *et al.* [6].

A. Cutting Forces Analysis

Figure 6 shows cutting force profile acquired from the simulation. In the analysis, a single peak value was taken and the comparison of different shear friction models and radial depths for AISI1055 shows in Figure 7 at cutting speed 75m/min.

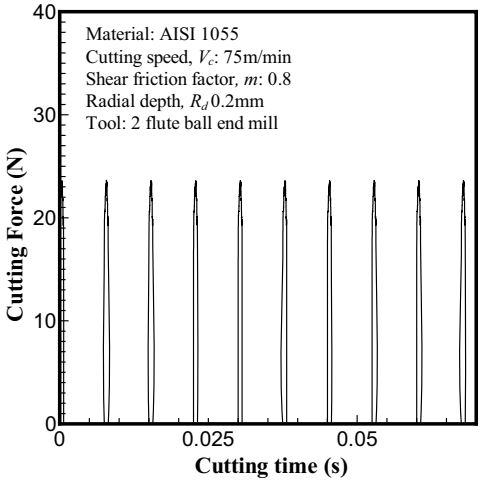

Figure 6: Cutting force profile

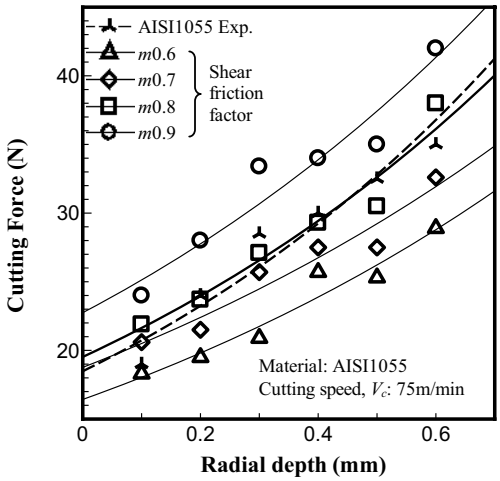

Figure 7: Effect of frictions model and radial depth on cutting force

From Figure 7, shear friction factor, m and radial depth, R_d shows a direct relation on cutting force. This is due to increasing frictional stress across the rake face and chip removal rate (mm^3/s). Shear friction factor 0.8 can be considered as the best shear friction model in estimating cutting force. This is due to lowest errors (10%) shown and with this shear friction model, high-precision simulation results that affiliated with cutting force such as cutting temperature could be acquired.

Identical simulation models were applied on machining process laser sintered material, LSMEρ9 with same shear friction factor of m0.8. The comparison between simulation and experimental results for AISI1055 and LSMEρ9 are shown in Figure 8. The figure shows that cutting force of AISI1055 is higher than LSMEρ9 at the same cutting rotational speed. This is because of LSMEρ9 is easy to deform due to lower Young Modulus (124GPa) compared to AISI1055 (250GPa).

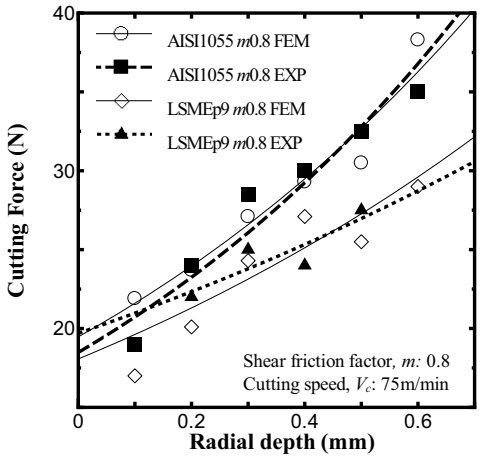

Figure 8: Effect of Young modulus and radial depth on cutting force

B. Cutting Temperature Analysis

Figure 10 shows the comparisons of estimated cutting temperature of AISI1055 and LSMEρ9 with experimental results after considering the cooling effect during the cutting process base on Eq. 5. From the figure, error below 5% is shown for FEM simulation of LSMEρ9 when compared to the experimental results. LSM shows a higher cutting temperature than AISI1055. This is due to the LSMEρ9's lower thermal conductivity (10 W/mK) than AISI1055 (53 W/mK). Heat becomes harder to conduct away from heat source for material with low thermal conductivity.

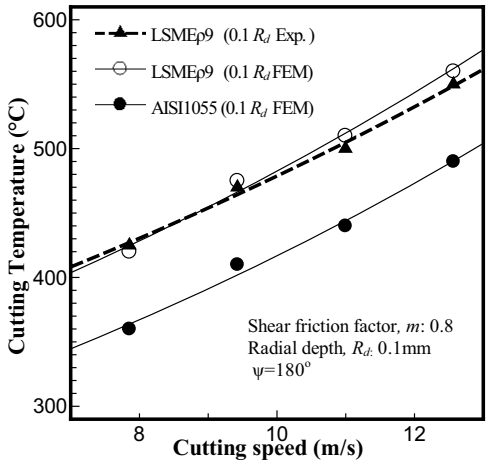

Figure 10: Effect of cutting speed on cutting temperature

Figure 11 shows the steady state analyses for temperature distributions inside the workpiece when machining both materials at 754m/min was done.

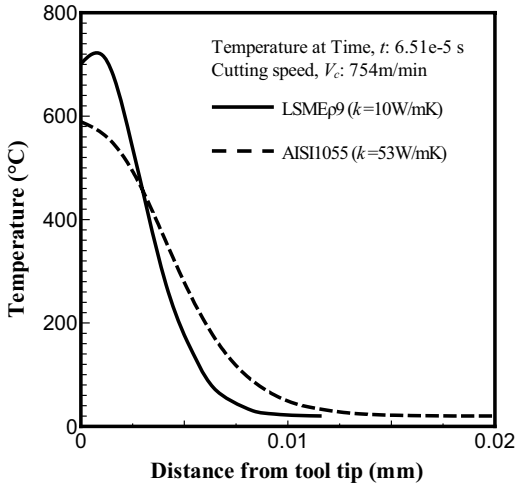

Figure 11: Temperature distribution comparison for different thermal conductivity

Workpiece temperature at the tool tip for LSMEρ9 is higher than AISI1055. However, cutting temperature decreases significantly for LSMEρ9 workpiece along the cross sectional compared to AISI1055 workpiece. This is due to the amount of heat travels inside LSMEρ9 workpiece is lower than AISI1055 in single unit time.

C. Different tool diameter analysis

Figure 12 indicates the comparison between estimated cutting temperatures with the experimental approach for ball end milling LSMEρ9 using 2mm and smaller diameter.

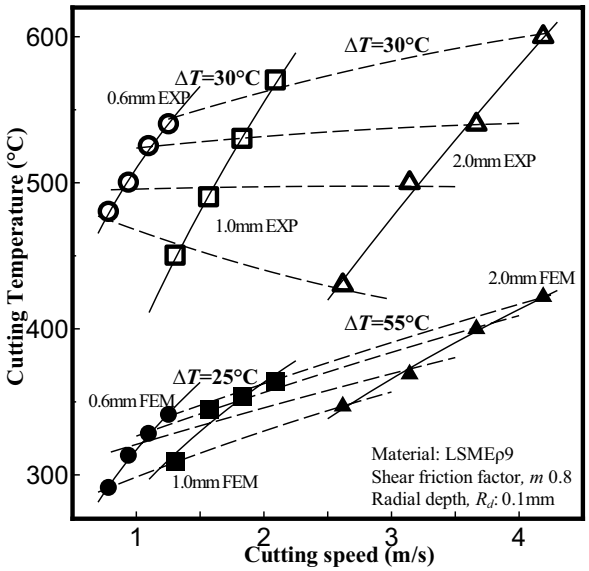

Figure 12: Comparison between estimated cutting temperatures with the experiment

The estimated cutting temperature displayed huge errors when compare with the experimental value by A. Yassin *et al.* [6]. This is due to the simulation were under the ideal process where other parameters such as tool wear are neglected.

Figure 13 indicates the relationship between cutting force and Merchant shear angle evolution with increasing cutting speed when machining LSMEρ9 for various tool diameters. The Merchant shear angle evolution is acquired from G. Sutter *et al.* [23] is shown in Eq. 6. θ_M is the Merchant shear angle, V is the cutting speed and α is the rake angle

$$\theta_M = (0.5\pi - 0.704V^{0.248} + \alpha)/2 \quad (6)$$

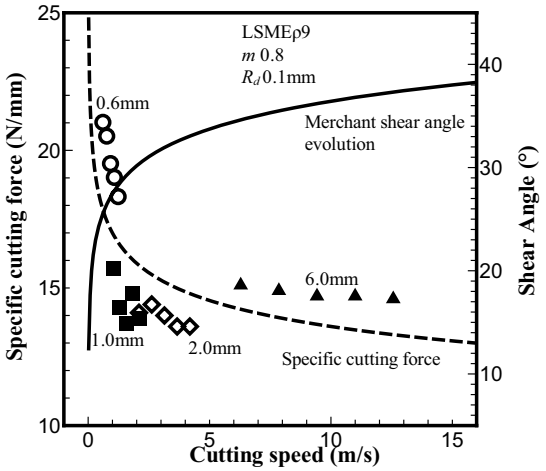

Figure 13: Effect of cutting speed on specific cutting force and Merchant shear angle evolution

From Figure 13, specific cutting force decreases when cutting speed increases due to increasing shear angle. However, at higher cutting speed, specific cutting forces show only a slight decrease. This phenomenon can be defined using Merchant shear angle evolution where the shear angle increase rate is higher at lower cutting speed but lower for cutting speed that is too high. It is long-familiar that shear angle has a direct influence on cutting force [24].

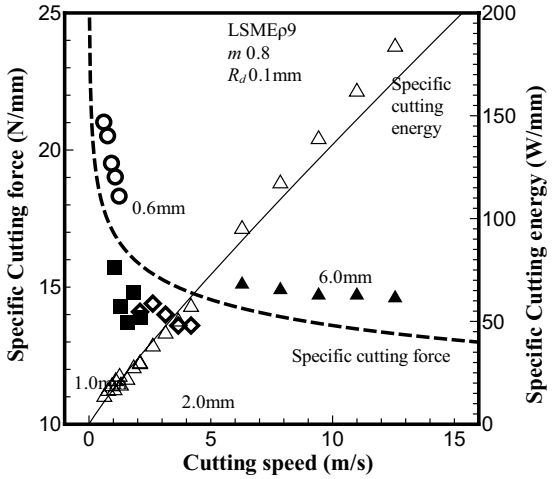

Figure 14: Effect of cutting speed on cutting force and cutting energy

Figure 14 shows the relationship between cutting force and cutting energy with increasing cutting speed during the FE analysis. Even though the cutting force is high at low cutting speed, the generated energy from the cutting process is small compared to cutting energy at higher cutting speed according to Eq. 3. Although obtaining experimental cutting forces in end milling is impossible due to measurement tool limitation, Figure 14 could explain the cutting force evolution and cutting energy at high cutting speed theoretically which the temperature value for lower diameter ball end mill should be smaller if the cutting process is ideal. [6].

Moreover, diameter of end milling operation that less than 6mm is considered as micro end milling operation, where the cutting tool suffered aggressive feed per tooth per radius compare to conventional milling operations, according to G. Newby *et al.* [25]. Furthermore, LSMEρ9 have high material hardness. This could increase tool wear rate for ball end mill less than 1.6mm and could contribute to increase cutting temperature during the experiment. Further investigation need to be done to explain this phenomenon such as effect of tool wear on cutting temperature using finite element analysis. Study on small ball end mill cutting performance with diameter less than 2.0mm is important to produce high precision mould.

V. Conclusion and Recommendation

In this study, machinability of laser sintered material (LSMeρ9) was studied by mean of cutting force and cutting temperature using FEM.

2D orthogonal cutting with thermo-mechanical plane strain model were applied. Constant shear friction factors range between 0.6-0.9 is used in the study and validated with the experimental results. Lowest error (10%) shown for estimated cutting force using *m*0.8. The cutting force increases with the increases in shear friction factor and radial depth of cut (R_d) due to increasing frictional stress and chip removal rate (mm^3/s).Cutting speed shows direct influence on cutting edge temperature due to increasing cutting energy. Lowest errors (5%) shown for estimated cutting temperature on AISI1055 and LSMEρ9 when validated with experimental results. AISI 1055 shows higher cutting force but lower cutting edge temperature than laser-sintered materials, LSMEρ9 due its higher Young modulus and lower thermal conductivity.

From the study, laser sintered material; LSMep9 can be considered having low machinability compared to mild steel due to higher cutting temperature. Plus with its high hardness, this characteristic could increase tool wear and roughness to the machined surface. FEM simulation results show decreasing cutting temperature when cutting tool diameter decreases. When comparing cutting tool temperature for less than 2mm diameter ball end mill, estimated cutting temperature shows large different compare to experimental results. This shown that other parameters such as cutting tool life and tool wear must be taken into account to investigated the errors.

VI. Acknowledgement

Author would like to show greatest appreciation to Ministry of High Education (KPT) of Malaysia and Universiti Malaysia Pahang (UMP) for funding the master study.

REFERENCES

[1] Dewes, R.C. and D.K. Aspinwall, *A review of ultra high speed milling of hardened steels.* Journal of Materials Processing Technology, 1997. 69(1-3): p. 1-17.

[2] King, D. and T. Tansy, *Rapid tooling: Selective laser sintering injection tooling.* Journal of Materials Processing Technology, 2003. 132(1-3): p. 42.

[3] Ramada, S. and P. Dickens, *Rapid tooling analysis of Stereolithography injection mould tooling.* International Journal of Machine Tools and Manufacture, 2007. 47 (5): p. 740-747.

[4] Kalpakjian, S. and S.R. Schmidt, *Manufacturing engineering and technology*. 4th ed. 2000: Prentice Hall International. 1148.

[5] Guzzle, B.U. and I. Lazuli, *An enhanced force model for sculptured surface machining.* Machining Science and Technology, 2004. 8(3): p. 431.

[6] A. Yassin , *Experimental Study on Machinability of Laser-sintered Material in Ball end Milling,* Phd Thesis, 2009, Kanazawa University

[7] L. Filice, F. Micari, S. Rizzuti, D. Umbrello, *Dependence Of Machining Simulation effectiveness On Material And Friction Modelling*, Machining Science and Technology, 12:3, 370

[8] T. Ozel, The *Influence of Friction Models On Finite Element Simulations of Machining*, Int. Journal of Tools and Manufacturing, 46(2006) 518-530

[9] E. Usui and Shirakashi, *Mechanics of Machining from Descriptive to Predictive Theory*, On the Art of Cutting Metals- 75 Years Later 7:13-55.

[10] J.S. Strenkowski, and J.T. Carroll, *A Finite Element Model of Orthogonal Metal Cutting*, Trans. ASME J. Eng. Ind., 107 (1985). 34

[11] J.P. Davim, and Maranhao, C. 2009. *A Study of Plastic Strain and Plastic Strain Rate in Machining of Steel AISI 1045 Using FEM Analysis*. Materials and Design 30: 160-165.

[12] J.P. Davim, C. Maranhao, M. J. Jackson, G. Cabral, J. Gracio, "*FEM analysis in high speed machining of aluminium alloy (Al7075-0) using polycrystalline diamond (PCD) and cemented carbide (K10) cutting tools*," Int. Journal, Advanced Manufacturing Technology, (2008), 39, 1093

[13] D. Umbrello, "*Finite element simulations of conventional and high speed machining of Ti6Al4V alloy*," Journal of Materials Processing Technology, Vol. 196, Issues 1-3, (2008) 79-87

[14] T. Ozel, T. Altan, "*Process simulation using finite element method - prediction of cutting forces, tool stresses and temperature in high speed flat end milling*," Int. Journal of Machine Tools & Manufacturing 40 (2000) 713-718

[15] T. Furumoto, T. Ueda, M.S. Abdul Aziz, A. Hosokawa, R. Tanaka, "*Study on reduction of residual stress induced during rapid tooling process – influence of heating conditions on residual stress*," Key Engineering Materials, 447-448: 785-789

[16] Kato S, Yamaguchi K, Yamada M (1972) "*Stress distribution at the interface between tool and chip in machining,*" Trans ASME J Eng Ind 94:683–689

[17] N. A. Abukhshim, P. T. Mativenga, M. A.Sheikh, "*Heat generation and temperature predicition in metal cutting: review and implications for high speed machining*," Int. Journal of Machine Tools & Manufacture 46(2006) 782-800

[18] R.T. Coelho, E. G. Ng , M. A. Elbestawi, "*Tool wear when turning hardened AISI 4340 with coated PCBN tools using finishing cutting conditions*," Int. Journal of Mahcine Tools and Manufacture Issue 2 - Volume 47(2007) 263-272

[19] N. A. Abukhshim, P.T. Mativenga, M. A. Sheikh, "*Investigation of heat partition in high speed turning of high strength alloy steel*," Int. Journal of Machine Tools & Manufacture 45(2005) 1687

[20] R.T. Coelho, E. G. Ng , M. A. Elbestawi, "*Tool wear when turning hardened AISI 4340 with coated PCBN tools using finishing cutting conditions*," Int. Journal of Mahcine Tools and Manufacture Issue 2 - Volume 47(2007) 263-272

[21] N. A. Abukhshim, P.T. Mativenga, M. A. Sheikh, "*Investigation of heat partition in high speed turning of high strength alloy steel*," Int. Journal of Machine Tools & Manufacture 45(2005) 1687

[22] A. Hosokawa, Z.P. Zhou, K. Yamada and T. Ueda, "*Studies on High-speed Milling with Small Ball End Mill: Temperature Distribution on Flank Face of Cutting Tool*," Journal of Japanese Society Precision Engineering, 70(12); 1527-1532

[23] G. Sutter, "*Chip geometries during high-speed machining for orthogonal cutting conditions*," International Journal of Machine Tools & Manufacture 45 (2005) 719-726

[24] E. Trent, P. Wright, 2000 " *Metal Cutting*" Fourth Edition, Butterworth Heinemann, US

[25] G. Newby, S. Venkatachalan, S.Y. Liang, "*Empirical analysis of cutting force constants in micro-end-milling operations*," Journal of Materials Processing Technology 192-193 (2007) 41-47